A view on phosphate ester photochemistry by time-resolved solid state NMR: intramolecular redox reaction of caged ATP

Cherepanov, A.V.; Doroshenko, E.V.; Matysik, S.C.; Vries, S. de; Groot, H.J.M. de

A view on phosphate ester photochemistry by time-resolved solid state NMR. Intramolecular redox reaction of caged ATP

Alexey V. Cherepanov,*[ab] Elena V. Doroshenko,[ab] Jörg Matysik,[a] Simon de Vries[b] and Huub J. M. De Groot[a]

Received 21st April 2008, Accepted 11th August 2008
First published as an Advance Article on the web 8th October 2008
DOI: 10.1039/b806677a

The light-driven intramolecular redox reaction of adenosine-5′-triphosphate-[P^3-(1-(2-nitrophenyl)-ethyl)]ester (caged ATP) has been studied in frozen aqueous solution using time-resolved solid state NMR spectroscopy under continuous illumination conditions. Cleavage of the phosphate ester bond leads to 0.3, 1.36, and 6.06 ppm downfield shifts of the α-, β-, and γ-phosphorus resonances of caged ATP, respectively. The observed rate of ATP formation is $2.4 \pm 0.2\ h^{-1}$ at 245 K. The proton released in the reaction binds to the triphosphate moiety of the nascent ATP, causing the upfield shifts of the ^{31}P resonances. Analyses of the reaction kinetics indicate that bond cleavage and proton release are two sequential processes in the solid state, suggesting that the 1-hydroxy,1-(2-nitrosophenyl)-ethyl carbocation intermediate is involved in the reaction. The β-phosphate oxygen atom of ATP is protonated first, indicating its proximity to the reaction center, possibly within hydrogen bonding distance. The residual linewidth kinetics are interpreted in terms of chemical exchange processes, hydrogen bonding of the β-phosphate oxygen atom and evolution of the hydrolytic equilibrium at the triphosphate moiety of the nascent ATP. Photoreaction of caged ATP *in situ* gives an opportunity to study structural kinetics and catalysis of ATP-dependent enzymes by NMR spectroscopy in rotating solids.

Introduction

Caged compounds are the photolabile probes, which contain biomolecules in the "chemically protected" inactive form. Irradiation of the probe with UV/visible light cleaves the cage moiety, releasing the biomolecule and triggering the process of interest. Phototriggering is a powerful experimental approach for targeting mechanistic problems in cellular systems biology, biochemistry and signal transduction.[1–10] The role of acetylcholinesterase in nerve-impulse transmission at cholinergic synapses has been studied by kinetic X-ray diffraction spectroscopy using caged arsenocholine as a product analogue.[11] Caged NADP and isocitrate derivatives have been employed in time-resolved Laue diffraction experiments for the spatio-temporal characterization of a transient enzyme-substrate complex of isocitrate dehydrogenase.[12] Very recently, we have applied phototriggering in the studies of molecular kinetics of Mg^{2+}-dependent adenylyl transfer catalyzed by DNA ligase from bacteriophage T4.[13,14] The reaction was initiated by release of Mg^{2+} from its complex with the photolabile EDTA cage derivative, DM-nitrophen. Low-temperature (LT) solid state NMR spectroscopy with magic angle spinning (LT-MAS NMR) was used to monitor chemical transformations in real time. The alternative way to trigger DNA ligase catalysis is to use caged ATP, adenosine-5′-triphosphate-[P^3-(1-(2-nitrophenyl)-ethyl)]ester (NPE-ATP), which contains the 2-nitrobenzyl phototrigger derivative at the γ-phosphate.[15] Caged ATP is a versatile tool in mechanistic studies of a broad range of cellular processes, the actin-activated ATPase reaction of myosin during muscle contraction and relaxation,[16–18] molecular rearrangements in protein chaperones,[19,20] kinesin-microtubule motility,[21,22] ATP hydrolysis in P-type ATPases,[23,24] action of mitochondrial ATP/ADP carrier,[25] *in vivo* intracellular Ca^{2+} mobilization,[26,27] and more. The goal of the present study is to show that caged ATP can be used in time-resolved LT-MAS NMR experiments for the photocontrolled release of ATP.

Light-driven hydrolysis of NPE-ATP proceeds *via* the intramolecular oxidation of a nitro benzyl ester forming a nitrosoketone, and involves 3 key reaction intermediates (Scheme 1). Excitation of the caged nucleotide **1a** leads to the formation of the *aci*-nitro intermediate **2a**, subsequent redox cyclization yields benzisoxazole **3a**, opening of the oxazole ring forms the hemiacetal intermediate **4a**, collapse of the hemiacetal releases nitrosoketone **6a**, ATP **7a**, and the proton. In solution, neutral **2a** and **3a** are in protolytic dissociation equilibrium with the anion species **2c** and **3c**. *Ab initio*, DFT,[28] semiempirical AM1 calculations[29] and experimental data[30] suggest that *aci*-nitro anion **2c** does not participate in cyclization. Using nanosecond laser flash photolysis and time-resolved infrared spectroscopy, it was shown that the rate of ATP release in solution at pH > 6 and ambient temperature is determined by the decay of the *aci*-nitro compound: the

[a] *Biophysical Organic Chemistry/Solid State NMR group, Leiden Institute of Chemistry, Faculty of Mathematics and Natural Sciences, Leiden University, Einsteinweg 55, 2333 CC Leiden, The Netherlands. E-mail: a.cherepanov@chem.leidenuniv.nl; Fax: +31715274603; Tel: +31715274539*
[b] *Section of Enzymology, Department of Biotechnology, Faculty of Applied Sciences, Delft University of Technology, Julianalaan 67, 2628 BC Delft, The Netherlands. E-mail: a.v.cherepanov@tudelft.nl; Fax: +31152782355; Tel: +31152781625*

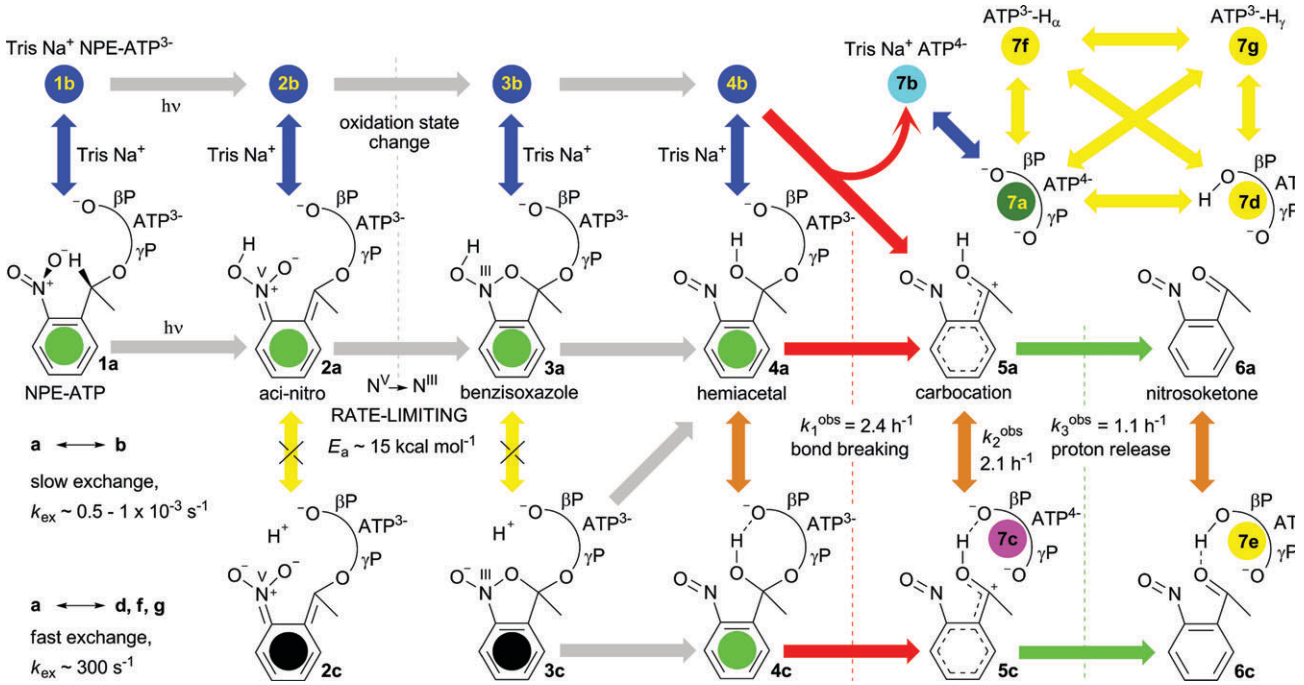

Scheme 1 Photoreaction of caged ATP: a view by ^{31}P time-resolved cryo-MAS NMR. Putative hydrogen bonds are indicated with dashed lines. ATP moiety is shown schematically, indicating positions of the oxygen atoms at β- and γ-phosphate and the formal charge of the triphosphate function. Apparent rate constants and the E_a value are shown for the reaction at 245 K in the solid state. Intermediates **1a–4a** and **6a** have been previously characterized in time-resolved studies of the reaction in solution as well as by molecular modeling. Putative intermediate **5a** and the Tris·Na^+-bound nucleotide species **1b–4b** and **7b** are observed in the present work. Scission of the phosphate ester bond is indicated with the red arrow. It causes downfield shifting of the phosphorus resonances of the nucleotide (Fig. 1). The proton release step is indicated with the green arrow. It causes the upfield shifts of the resonances of the nascent ATP. Chemical steps that are invisible by ^{31}P NMR are indicated with the gray arrows. Binding of Tris·Na^+ to the nucleotide is indicated with the blue arrows. It occurs in the slow exchange regime, with the estimated exchange rate $k_{ex} \sim 0.5\text{-}1 \times 10^{-3}$ s^{-1}. Under these conditions, the exchanging species are observed as two separate sets of signals. The yellow arrows indicate proton transfer steps, which occur under the fast exchange conditions, with $k_{ex} \sim 300$ s^{-1}. In this case, the signals of the four exchanging species (**7a**, **7d**, **7f**, **7g**) converge to a single set of resonances after completion of the reaction. During the reaction, these resonances shift upfield following an increase in [H^+]. The brown arrows indicate the weak hydrogen bonding between the O_β and the hydroxyl hydrogen in **4c** and **6c**. Broadening of the βP resonance can be interpreted in terms of this exchange process. The violet arrow indicates formation of a stronger hydrogen bond between the O_β of **7c** and the hydroxyl hydrogen of **5c**. The ~0.1 ppm upfield "burst shift" of the βP resonance of the nascent ATP can be explained by this process. The colors of the ^{31}P-containing species correspond to different sets of chemical shift values summarized in Table 1.

oxidative cyclization step **2a** → **3a** is rate-limiting;[28] both benzisoxazole and hemiacetal intermediates are transient, hydrolyzing as quickly as they are formed.[31]

In this work, we have used LT-MAS ^{31}P NMR to study the photoreaction of caged ATP at 245 K in the solid state. The inherently high NMR chemical shift sensitivity allowed resolving collapse of the hemiacetal intermediate with concomitant release of the proton and observing the chemical exchange processes, which include hydrogen bonding interactions and evolution of the protolytic equilibrium. The detailed kinetic analyses of the isotropic chemical shift, residual linewidth and intensity changes lead to a model where the initial light excitation step is followed by two parallel cascades of dark reactions interconnected by chemical equilibria. The present study opens a new field of application of NPE-ATP in protein chemistry and catalysis, where it can be used for the structural characterization of enzyme-catalyzed chemical reactions by time-resolved solid state NMR spectroscopy.

Experimental

Adenosine-5′-triphosphate-[P^3-(1-(2-nitrophenyl)-ethyl)]ester disodium salt was purchased from Calbiochem (#119127) and used without further purification. Solid ATP·Na_2 and 0.5 M solution of Tris(2-carboxyethyl)phosphine (TCEP), pH = 7 were obtained from Sigma Aldrich. For MAS NMR experiments, the 4-mm zirconia rotors from Bruker were used. Care was taken to avoid the contact of the nucleotide solutions with the partially stabilized zirconia ceramics (MgO ZrO_2) of the rotor. Diluted HCl causes corrosion and disintegration of zirconia at elevated temperature and pressure, dissolving MgO.[32] Mg^{2+} in solution binds ATP and subsequently the proton, forming the H·ATP·Mg^{1-} complex, which has the apparent ionization constant $pK_{a1} \sim 3.6$, similar to the ATP complexes with the other divalent cations.[33] To separate zirconia from the solution, the inner surface of the rotor was coated with parafilm (Pechiney Plastic Packaging Company) prior to loading the sample. The rotor was placed vertically in the solid aluminium holder in the furnace and heated to 420–430 K. A tightly compressed parafilm roll (2–3 mm diameter, 10–15 mm length) was inserted in the rotor and allowed to melt for 5–10 min. The excess of parafilm was forced out of the rotor with the 3.8-mm-diameter stainless steel rod, leaving a thin glue-like layer of melted parafilm on the inner surface of the rotor. The hot rotor with the holder was removed from the furnace and left at room temperature for

slow cooling. A solution of 10 mM caged ATP was prepared in 77 mM Tris-HCl, pH = 7.5 (293 K) and 2 mM Tris-(2-carboxyethyl)phosphine (TCEP) at 277 K in the dark, transferred to the rotor (*ca.* 0.7 mg of solid ATP, 1 μMol), stored on ice and loaded in the spectrometer within 2 h after preparation. The sample was freeze-quenched in the spectrometer at 1 kHz spinning frequency (12.5 m s^{-1} linear rate) and a temperature ramp rate of 10–20 K min^{-1}, providing complete solidification. Proton-decoupled ^{31}P MAS NMR spectra were recorded at a frequency of 303.606 MHz with a wide bore Bruker Avance DMX 750 spectrometer using LT MAS probe modified for the light-driven experiments.[34,35] The chemical shift positions of the nucleotides were measured relative to $(NH_4)_3PO_4$. Each spectrum contained 512 scans recorded at 245 K and 8 kHz spinning rate with the recycle delay of 0.25 s (spectrum acquisition time, expt = 2.4 min). The optical setup, which was used in this work is equipped with a 1 kW Xenon arc light source. The measured illuminance in the MAS NMR rotor is 100–120 kLux: 1 μE of photons (in the 380–780 nm wavelength range) is delivered every 30 sec per 1 μMol of NPE-ATP. The light was turned on after acquisition of the 5th spectrum. Aqueous solutions of 10 mM ATP, 30 mM NaOH, 2 mM TCEP (A), 10 mM ATP, 77 mM Tris base, 2 mM TCEP (B), 77 mM Tris base, 2 mM TCEP (C), and 77 mM Tris base (D) were titrated by addition of HCl. For NMR experiments, the aliquots of solution (B) were withdrawn at different pH values and stored at 77 K until use. The NMR measurements were performed at 225 and 245 K; the sample was equilibrated at each temperature for 30 min before starting the acquisition. Each spectrum

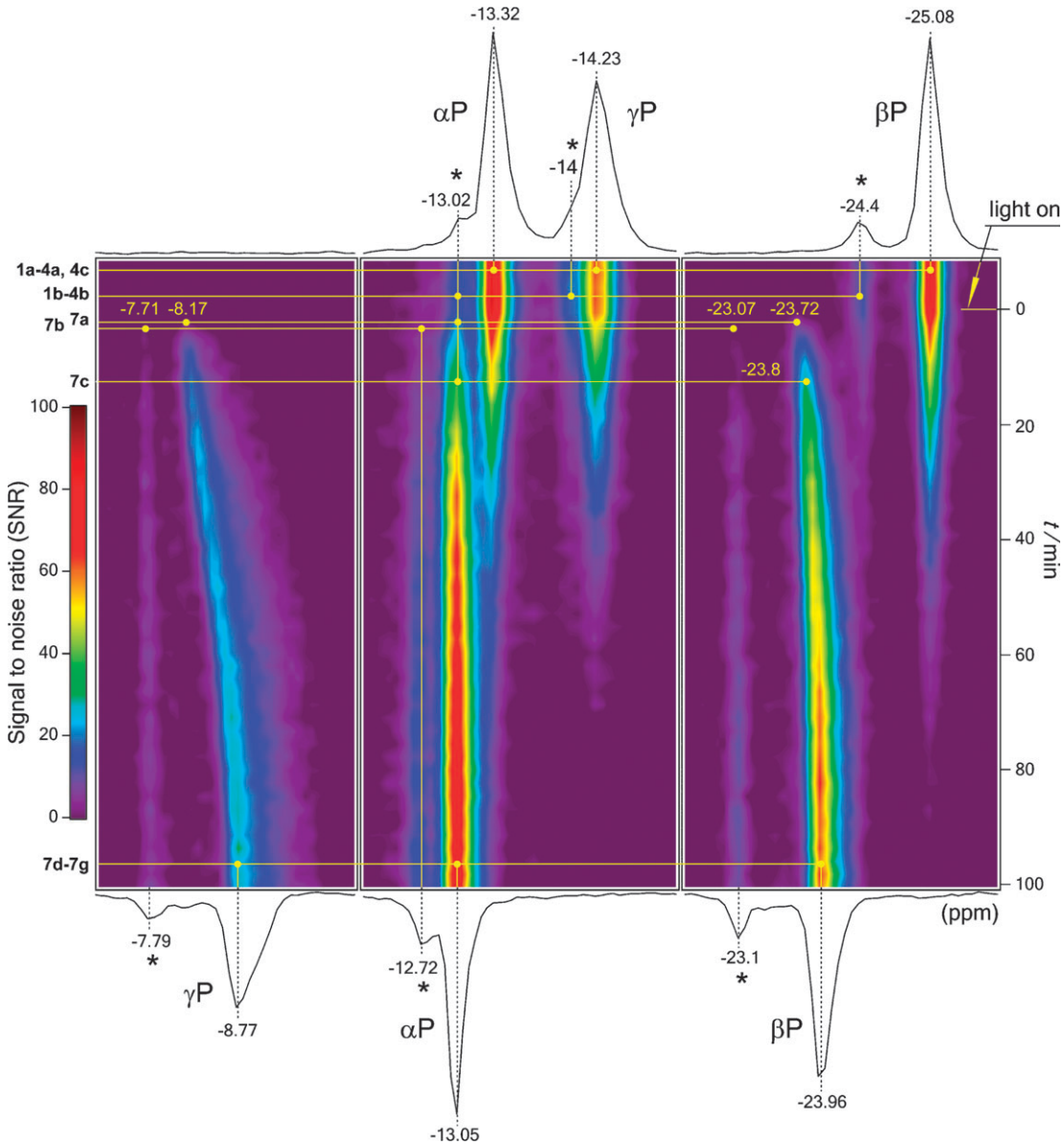

Fig. 1 The ^{31}P signal-to-noise ratio (SNR)-time spectral density plot (SDP) of the photoreaction of caged ATP. The spectral changes are correlated to the reaction intermediates abbreviated in Scheme 1. The resonances of Tris·Na·nucleotide complexes are marked with an asterisk. The color scale shows the SNR of the proton decoupled ^{31}P MAS NMR resonances.

contained 5400 scans (expt = 25 min). Igor Pro software (Wavemetrics) was used for data analysis, including deconvolution of the spectrum in Fig. 1.

Results and discussion

Time-resolved solid state NMR studies were performed at low temperatures with magic angle spinning. The experiment included: (i) preparing a liquid sample of caged ATP; (ii) freeze-quenching the sample in the NMR spectrometer at 245 K; (iii) triggering the reaction by illumination; and (iv) monitoring chemical transformations in real time. The reaction chemistry at the γ-phosphorus of NPE-ATP is reflected in the proton-decoupled ^{31}P MAS NMR spectral density plot (SDP) shown in Fig. 1. The spectral changes are correlated to the reaction intermediates in Scheme 1. The isotropic chemical shift values (δ) of the intermediates are summarized in Table 1. The resonances of NPE-ATP shift downfield during cleavage of the NPE ester bond, release of the photoactive protecting group (ppg) and formation of ATP. The shift of the γ-phosphorus atom harboring the cage moiety is the largest, 6.06 ppm. The β-phosphorus atom, which is located further away from ppg shifts by 1.12 ppm; the shift of the remote α-phosphorus atom is the smallest, 0.3 ppm. Four distinct species are observed throughout the reaction, indicating that the triphosphate moieties of NPE-ATP and ATP both exist as mixtures of two conformers that exchange slowly on the time scale of the NMR experiment. Assuming that the relaxation times of the conformers are similar, the estimated conformer ratio is 0.2:0.8 at 245 K and pH = 7.5. The resonances of the minor species are shifted downfield in both caged and nascent ATP (Fig. 1, peaks marked with the asterisk). The conformer ratio decreases with both pH and temperature and the minor species dissapear at pH < 3 and/or T < 225 K. The exchange rate of $k_{ex} \sim 0.5–1 \times 10^{-3}$ s^{-1} could be estimated in the temperature jump experiment by following the redistribution of the conformers after a rapid drop of the temperature by 10 degrees.

Table 1 The isotropic chemical shifts for the observed ^{31}P signals of the reacting species

Intermediate	$\delta_{\alpha P}$	$\delta_{\beta P}$	$\delta_{\gamma P}$
1a, **2a**, **3a**, **4a**, **4c** (green)	−13.32	−25.08	−14.23
1b, **2b**, **3b**, **4b** (blue)	−13.02	−24.4	−14
2c, **3c** (black)	ND		
7a (dark green)	−13.02	−23.72	−8.17
7b (light blue)	−12.72	−23.07	−7.71
7c (violet)	−13.02	−23.8	−8.17
7d, **7e**, **7f**, **7g** (yellow)	−13.05	−23.96	−8.77

ND—not detected; colours refer to Scheme 1.

The origin of the minor species derives from the Tris buffer, which readily forms binary and ternary complexes with metal cations and ATP. The dissociation constants vary in the range between 280 μM and 0.2 M, depending on the metal type, pH, ionic strength and temperature.[36] In Fig. 1, the minor species can be attributed to the ternary Tris·Na·nucleotide complexes. Even without Tris, Na^+ forms complexes with ATP, causing downfield shifts of the α-, β- and γ-phosphorus resonances by 0.05, 0.16 and 0.26 ppm, respectively.[37] From the LT-MAS NMR data of the Tris·Na complexes with NPE-ATP or ATP presented here, it is difficult to estimate their dissociation constants in solution: at low temperature the Bjerrum ion-pairing and aggregation of ionic species increases, which is often enhanced by the water–ice phase transition and the structural mobility of the ice lattice. At the conditions of our NMR experiment (frozen aqueous solution at 245 K and pH = 7.5), the dissociation constants for the Tris·Na complexes with NPE-ATP or ATP can be estimated as $K_d \sim 0.3$ M.

For NPE-ATP, the β-phosphate moiety is the main point of contact of the nucleotide with the buffered sodium cation: the 0.68-ppm difference between the chemical shift of the βP resonance ($\delta_{\beta P}$) in Tris·Na·NPE-ATP^{2-} and NPE-ATP^{3-} is the largest compared to the similar $\Delta\delta$s of the α- and γ-phosphorus resonances, 0.3 and 0.23 ppm, respectively (*cf.* Table 1). The NPE cage sterically hinders the γ-phosphate group from interacting with Tris·Na^{1+}: $\Delta\delta_{\gamma P}$ increases almost two-fold upon the release of ppg, 0.23 ppm for Tris·Na·NPE-ATP^{2-} *vs.* 0.38 ppm for Tris·Na·ATP^{3-}. The interaction with α-phosphate remains the same, while the

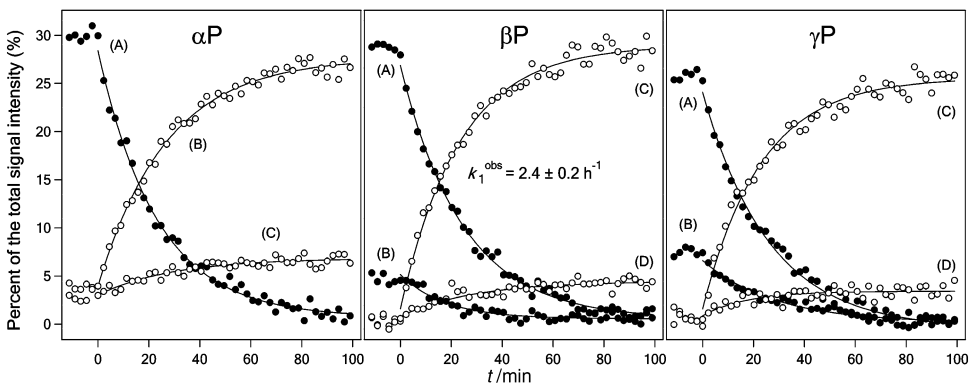

Fig. 2 Kinetic traces of the photoreaction of caged ATP obtained from deconvolution of the SDP in Fig. 1 and integration of the individual spectral components. (●) – the intensity values of the ^{31}P resonances of caged ATP; (○) – *ibid.* of the nascent ATP. **αP**. (A) – **1a–4a**, **4c** at −13.32 ppm. (B) – **7a**, **7c**, **7d–7g** between −13.02 and −13.05 ppm. (C) – **7b** at −12.72 ppm. **βP**. (A) – **1a–4a**, **4c** at −25.08 ppm. (B) – **1b–4b** at −24.4 ppm. (C) – **7a**, **7c**, **7d–7g** between −23.72 and −23.96 ppm. (D) – **7b** between −23.07 and −23.1 ppm. **γP**. (A) – **1a–4a**, **4c** at −14.23 ppm. (B) – **1b–4b** at −14 ppm. (C) – **7a**, **7c**, **7d–7g** between −8.17 and −8.77 ppm. (D) – **7b** between −7.71 and −7.79 ppm.

interaction with β-phosphate slightly weakens, with the $\Delta\delta_{\beta P}$ = 0.61 ppm for Tris·Na·ATP^{3-} *vs.* 0.68 ppm for Tris·Na·NPE-ATP^{2-} species.

Deconvolution of the SDP to the individual spectral components shows a monophasic exponential process with the observed rate constant k_1^{obs} = 2.4 ± 0.2 h^{-1} (Fig. 2). Both free and buffered sodium-nucleotide complexes display the same rate of conversion, indicating that the configuration of the triphosphate chain does not influence the light-induced bond alteration at the NPE moiety. The exponential kinetics indicate that the reaction does not occur in the light-limiting regime; otherwise, the product formation traces in Fig. 2 would be linear, following the zero-order steady-state conditions. To verify that the reaction kinetics does not depend on the light intensity, we have decreased the illuminance 7.1-fold and repeated the measurements. The k_1^{obs} decreased 1.7-fold, to 1.4 ± 0.2 h^{-1} and the product formation trace linearized. From this value, the rate of photoexcitation under full illuminance conditions was estimated as k_{phot} ~ 10 h^{-1}, 4.2-fold higher than the k_1^{obs} of ATP release at 245 K. The decrease of the temperature to 240 K under full illuminance conditions slowed down the reaction twofold, to 1.2 ± 0.2 h^{-1}. Assuming the Arrhenius reaction behavior, the activation energy for ATP release in ice can be estimated as E_a ~ 15 kcal mol^{-1}, similar to that in solution, 14.8 kcal mol^{-1}.[38,39] Taking the k_1^{obs} = 218 ± 33 s^{-1}[40,41] at pH = 7 and 295 K and accounting for the rate dependence on pH[28] and temperature,[38,39] the rate constant in solution at pH = 8 and 273 K can be estimated as k_1^{obs} ~ 2.8 s^{-1}. At 273 K in ice, the same value can be calculated as k_1^{obs} ~ 64 h^{-1}, taking the k_1^{obs} = 2.4 ± 0.2 h^{-1} at 240 K and the 15-kcal mol^{-1} activation energy. It is unlikely that the mechanism of the rate-limiting oxidative cyclization step **2a** → **3a** or the structure of the reaction intermediates would differ in ice from that in solution: the enthalpic component (E_a) of the rate constant is similar in both phases. On the other hand, ice lattice might impose an entropic penalty on the functional motions of the reacting groups. Such a loss of activation entropy could lead to the estimated ~160-fold drop of the k_1^{obs} value during water–ice phase transition.

The analyses of the ^{31}P LT-MAS NMR data recorded for ATP in the pH range between 1 and 9 demonstrate the sensitivity of the ATP phosphorus nuclei to the protonation state of the phosphate oxygen atoms (Fig. 3, Table 2). ATP has four ionizable phosphate groups and the adenine ring, which can be protonated at the N1 position.[42] In strongly acidic solutions ATP exists as a cation H_5·ATP^{1+}. At pH ~ 9, the starting point in our titration experiments, ATP is present in the fully ionized form ATP^{4-}. Binding of the first proton to the triphosphate moiety of ATP^{4-} results in the upfield shifts

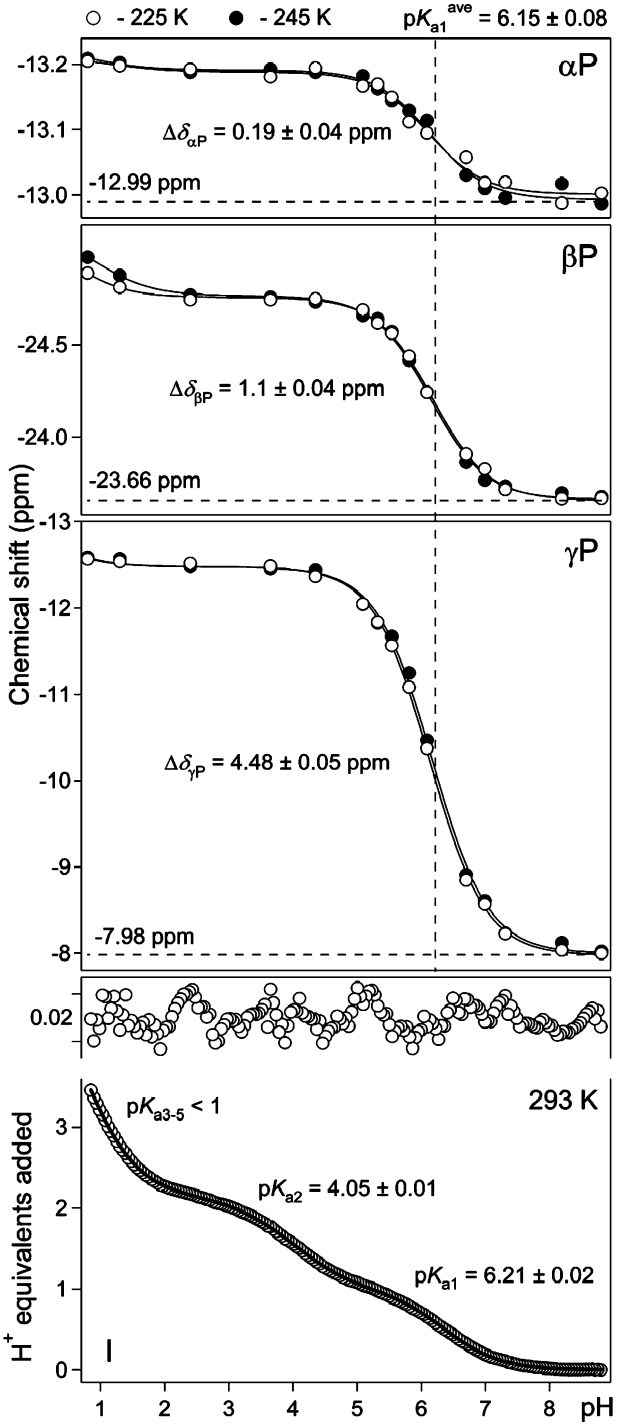

Fig. 3 pH titration curves recorded at 293 K in solution by using the glass electrode (**I**) and at low temperatures in the solid state by using ^{31}P LT-MAS NMR (**α**–, **β**–, **γP**). NMR spectra were recorded as described in the Experimental section. Empty circles in panels **α**–, **β**–, **γP** refer to the isotropic chemical shifts (δ) of the corresponding ATP ^{31}P resonances determined at 225 K; solid circles—*ibid.* at 245 K. $\Delta\delta$ and apparent pK_a values were calculated by treating the titration curve of a polyprotic acid (H_5ATP^{1+}) as a superposition of those for monoprotic acids having the corresponding K_as. Traces in panels **α**–, **β**–, **γP** were fitted with a linear sum of the modified Henderson–Hasselbalch equation, $pH = pK_a = \log\frac{\delta_{max}-\delta}{\delta-\delta_{min}}$ where δ is the observed chemical shift, δ_{max} is the shift under acidic conditions and δ_{min} is the shift under basic conditions for each protonation site. For fitting of the titration curve in panel **I**, the log part of the equation was rewritten as $\log\frac{\Delta-H^+_{eq}}{H^+_{eq}}$ where H^+_{eq} is the equivalent fraction of added acid and Δ is the fraction required to pass through a single equivalence point (Δ = 1 for p$K_{a1,2}$ and Δ = 3 for pK_{a3-5}). Fitting residuals are shown above the titration curve. To exclude the protonation of the Tris base for clarity of the presentation, the difference trace B minus C (*cf.* Experimental section) is shown in panel **I**, which reflects only the ionizable groups of ATP.

Table 2 The isotropic chemical shifts and the apparent pK_a values for the ionized forms of ATP and Tris·Na·ATP

Compound	$\delta_{\alpha P}$	$\delta_{\beta P}$	$\delta_{\gamma P}$	pK_a
ATP^{4-}	−12.99	−23.66	−7.98	
$H{\cdot}ATP^{3-}$	−13.19	−24.76	−12.48	[a]6.15 ± 0.08/ [b]6.21 ± 0.02
$H_2{\cdot}ATP^{2-}$	−13.19	−24.76	−12.48	4.05 ± 0.01
$H_3{\cdot}ATP^{1-}$	<-13.22[c]	<-25.1[c]	<-12.6[c]	<1[c]
$Tris{\cdot}Na{\cdot}ATP^{3-}$	−12.72	−23.09	−7.68	
$Tris{\cdot}Na{\cdot}ATP{\cdot}H^{2-}$	−12.86	−23.78	−11.3	5 ± 0.3

[a] Determined at 225 and 245 K in the solid state. [b] Measured at 293 K in solution. [c] Upper limit values.

of the γ- and βP resonances by 4.48 and 1.1 ppm, respectively; the upfield shift of the remote α-phosphorus atom is the smallest, 0.19 ppm. These values are essentially the same at 225 and 245 K. The situation resembles the case of NPE-ATP, where a bound proton, similarly to the covalently attached NPE moiety increases the electronic polarization at the phosphorus nucleus, thereby decreasing its resonance frequency. Polarization decays with the inverse square of the distance from the proton binding site, which can be noted by comparing the $\Delta\delta$ values of the individual ^{31}P resonances (Fig. 3). Judging these values, the first proton should bind to the γP phosphate of ATP^{4-}, which is also electrostatically favorable, since it carries the highest negative charge. The apparent ionization constant for $H{\cdot}ATP^{3-}$ is the same at 225 and 245 K, pK_{a1} = 6.15 ± 0.08. It is similar to the value determined at 293 K in solution, pK_a = 6.21 ± 0.02 (Fig. 3-I) and the values reported in the literature.[43,44] $Tris{\cdot}Na{\cdot}ATP^{3-}$ also binds the proton to the γ-phosphate, forming $Tris{\cdot}Na{\cdot}ATP{\cdot}H^{2-}$ with the pK_{a1} = 5 ± 0.3. The titration cannot be completed; the proton seem to compete with $Tris{\cdot}Na^+$ in the dynamic equilibrium $Tris{\cdot}Na{\cdot}ATP{\cdot}H^{2-}$ = $Tris{\cdot}Na^+ + ATP{\cdot}H^{3-}$; $Tris{\cdot}Na^+ + H^+ = Tris{\cdot}H^+ + Na^+$, leading to the gradual decrease of the ^{31}P resonances of $Tris{\cdot}Na{\cdot}ATP{\cdot}H^{2-}$ and dissapearance of the signal at pH < 3.

The second proton binds to the N1 atom of the adenine ring with the pK_{a2} = 4.05 ± 0.01 (Fig. 3-I, Table 2), which matches the earlier reported values.[42–44] Binding of this proton is invisible in ^{31}P NMR experiments (Fig. 3), indicating no interaction between the N1–H^+ form and the ATP phosphate oxygen atoms. The three remaining proton-binding sites at the triphosphate chain ionize at pH below 1. The corresponding equivalence points could not be resolved with the glass electrode, the response of which does not follow that of the hydrogen electrode at low pH. In the NMR experiments, we could observe weak upfield shifts of all three ^{31}P resonances of ATP at low pH values, which imply binding of the third proton, forming $H_3{\cdot}ATP^{1-}$. Judging by the size of the shifts (Fig. 3, Table 2), the third proton binds to the β-phosphate-oxygen anion.

In the case of NPE-ATP, cleavage of the NPE ester bond is accompanied by a release of one proton equivalent. This process is detected by ^{31}P NMR as a shift of the ^{31}P signals of the nascent ATP (Fig. 4-II). The α- and γP resonances shift upfield during the reaction by 0.03 and 0.71 ppm, respectively, corresponding to an effective protonation of 0.16 H^+ (Fig. 4-II αP-1, γP-1). The fractional protonation values are calculated from the $\Delta\delta$ values shown in Fig. 3. After the release of the proton, the pH in the frozen reaction mixture decreases from 7.5 to 6.8, which can be calculated from the shifts of the γ- and αP resonances and the titration curves in Fig. 3. The same decrease for 0.7 pH units occurs in solution B at 293 K and pH = 7.5 after addition of one proton equivalent. This relatively small value reflects the buffering capacity of the Tris base. In the presence of ATP alone, pH would decrease for 2.5 units, from 7.5 to 5 (Fig. 3-I). The 0.29-ppm upfield shift of the βP resonance is higher than expected from the pH-jump only, indicating the presence of an additional polarizing interaction between the βP oxygen atom and ppg. The residual interaction of the nascent ATP^{4-} (**7a**) with the cleaved ppg in the solid state is evident from the difference between the chemical shifts of **7a** (Table 1) and ATP^{4-} prepared in the absence of ppg (Table 2). All resonances of **7a** are shifted upfield compared with ATP^{4-}. The size of the shifts decreases in the sequence γP > βP > αP.

Upon release of the proton, the phosphate resonances of the nascent $Tris{\cdot}Na{\cdot}ATP^{3-}$ complex display minor upfield shifts, the γP ~ 3-fold more than the βP (Fig. 4-II βP-2, γP-2), indicating that $Tris{\cdot}Na^{1+}$ shields the triphosphate moiety from the proton, perhaps by sandwiching between the NPE phototrigger and the phosphate groups. The shifts match the values estimated by using the pK_{a1} = 5 ± 0.3 for $Tris{\cdot}Na{\cdot}ATP{\cdot}H^{2-}$ (Table 2) and the pH decrease from 7.5 to 6.8. The phosphorus resonances of caged ATP do not shift significantly during the reaction (Fig. 4-I), indicating that in the solid state at 245 K **2c** and **3c** are not formed, *i.e.*, that the proton is not released *before* the ester bond is broken (Scheme 1).

The sequence of ATP protonation events is somewhat puzzling; the first phosphate group to encounter the proton is *beta*: the βP resonance experiences a "burst" upfield shift during the first 10 min of the reaction ($\Delta\delta$ = 0.08 ppm, k_2^{obs} = 2.1 ± 0.2 h^{-1}, Fig. 4-II βP-1). Subsequently, the shifting rate slows down ~2-fold, entering a single-exponential phase ($\Delta\delta$ = 0.21 ppm, k_3^{obs} = 1.1 ± 0.1 h^{-1}), during which the protolytic equilibrium at the triphosphate moiety is established (Scheme 1). The "burst" shift indicates that the β-phosphate oxygen atom interacts with ppg, possibly by forming a hydrogen bond with the hydroxyl hydrogen at the exocyclic C_α position (Scheme 1, **5c**,**7c**). The sigmoidal protonation kinetics at the γ-phosphate, with a distinctive lag phase at the time of the βP protonation burst, supports this conclusion (Fig. 4-II γP-1). On the other hand, hydrogen bonding of the β-phosphate oxygen is not essential for the bond making-and-breaking: the Tris·Na·NPE-ATP complex shows the same rate of ATP release (Fig. 2), even though the triphosphate moiety is separated from ppg by $Tris{\cdot}Na^{1+}$. Thus, the β-phosphate oxygen atom of ATP appears to be a mere NMR sensor of the reaction events, rather than an active participant.

The k_3^{obs} for the protonation of ATP (1.1 ± 0.1 h^{-1}) is smaller than the k_1^{obs} for the cleavage of the NPE ester bond (2.4 ± 0.2 h^{-1}). Binding of the proton is observed as a shift of the resonances of the nascent ATP and *not* of its caged precursor. The overall protonation rate is determined by two

processes, proton release from the benzylic alcohol and diffusion of the proton to the triphosphate moiety. The intersite diffusion time can be estimated as $\tau = d^2/D$, where d is the separation distance and D is the proton diffusion coefficient. At 245 K, the self-diffusion coefficient for the proton in hexagonal ice Ih is $\sim 3 \times 10^{-16}$ m^2 s^{-1}.[45] The maximal separation distance is ~ 10 Å, taking the total length of four P–O, two C–O and one O–H bonds. The resulting $\tau \sim 3 \times 10^{-3}$ s gives a diffusion rate constant, which is 6 orders of magnitude higher than k_3^{obs}. It is clear that the rate of

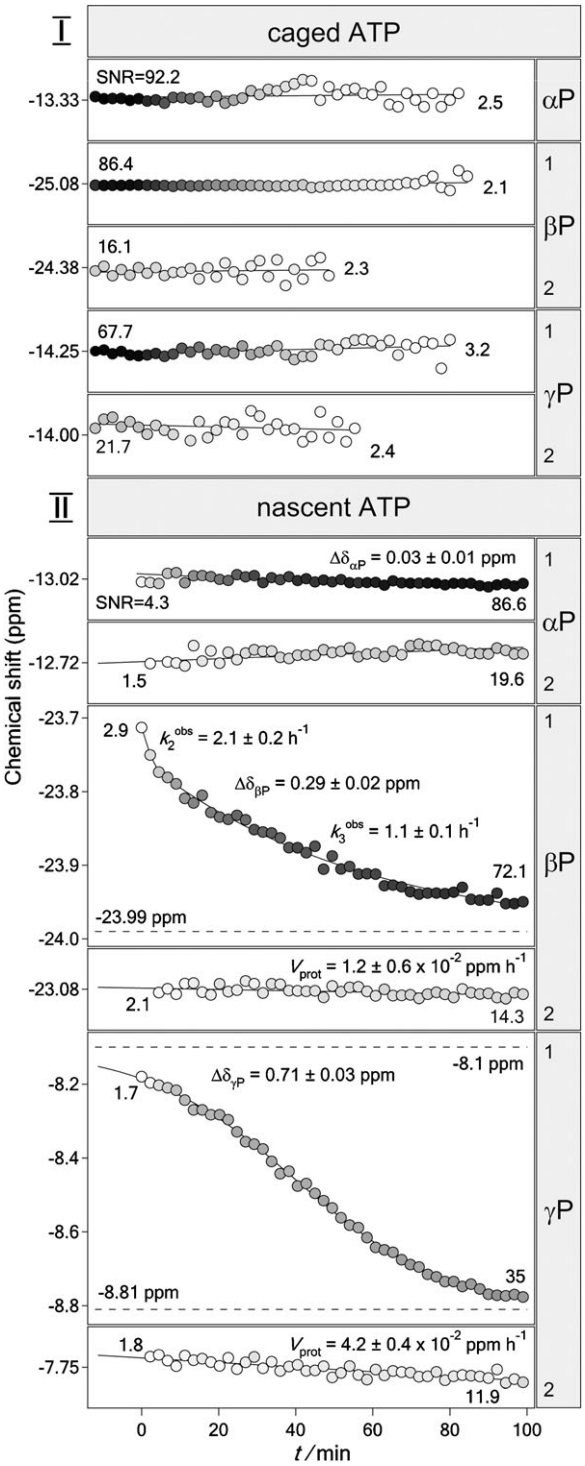

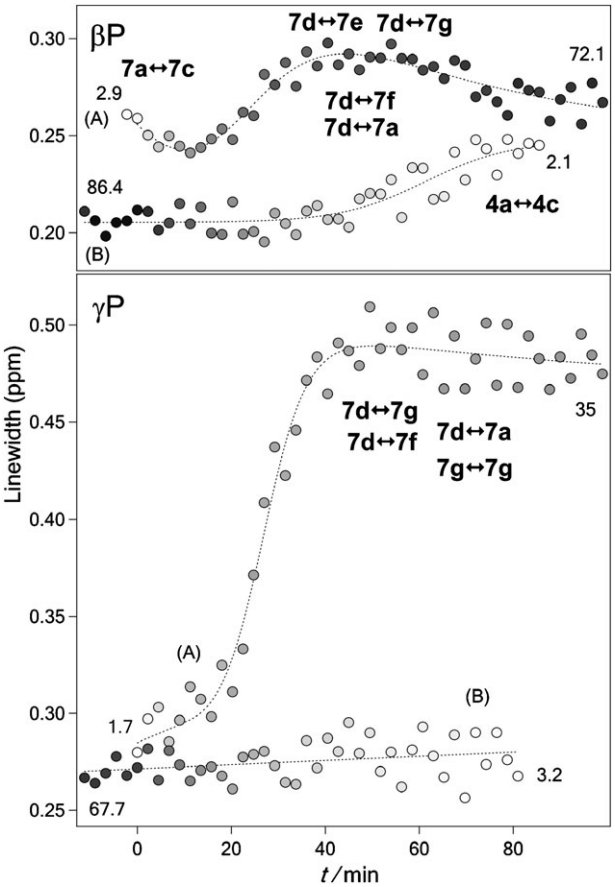

Fig. 5 ^{31}P residual linewidth kinetic traces of the photoreaction of caged ATP. The gray shading of each data point shows the SNR value of the corresponding peak represented on a gray scale from 0 to 93. The values at the beginning and end of each trace show the SNR value for the first and last point, respectively. Kinetic traces are correlated to the chemical exchange events shown in Scheme 1.

protonation of ATP is determined by the formation of nitrosoketone **6a** and not by proton diffusion. This implies a sequential order of reaction events: first, the bond is cleaved (2.4 ± 0.2 h^{-1}) and second, the proton is released (1.1 ± 0.1 h^{-1}). An additional reaction intermediate, the doubly stabilized 1-hydroxy,1-(2-nitrosophenyl)ethyl carbocation **5a**, in which the ester bond is broken, but the proton is not yet released, is proposed to participate in the reaction. This intermediate is ^{31}P NMR silent, but the co-formed ATP^{4-} (**7a**) has the characteristic β- and γP resonances at −23.72 and −8.17 ppm, respectively (Fig. 1, Table 1). In our setup, the photoreaction is driven by a continuous illumination of the NMR sample. Under these conditions, hemiacetal **4a** might

Fig. 4 ^{31}P chemical shift kinetic traces of the photoreaction of caged ATP. The gray shading of each data point shows the SNR value of the corresponding peak represented on a gray scale from 0 to 93. The values at the beginning and end of each trace show the SNR value for the first and last point, respectively. Panel I—NPE-ATP. The scale of each graph is 0.1 ppm. **αP**. **1a–4a**, **4c**; **βP**. **1**—**1a–4a**, **4c**; **2**—**1b–4b**; **γP**. **1**—**1a–4a**, **4c**; **2**—**1b–4b**; Panel II—nascent ATP. **αP**. **1**—**7a**, **7c**, **7d–7g**; **2**—**7b**. The scale of the graphs is 0.1 ppm. **βP**. **1**—**7a**, **7c**, **7d–7g**; **2**—**7b**. The scale of II βP-2 is 0.1 ppm. **γP**. **1**—**7a**, **7c**, **7d–7g**; **2**—**7b**. The scale of II γP-2 is 0.1 ppm.

decompose to **5a** and **7a** *via* heterolytic photofragmentation, similar to the reaction of the arylmethyl phosphate esters, where the electron-deficient benzyl cation paired with the departing phosphate ion is a key photolytic intermediate.[46,47]

The ^{31}P residual linewidth ($W_{1/2}$) kinetics of the photoreaction are shown in Fig. 5. The most affected resonance is γP of ATP. In the first 40 min its linewidth increases nearly two-fold (Fig. 5 γP-A). The $W_{1/2}^{\gamma P}$ trace has a sigmoid shape, which is more pronounced than for the γP chemical shift trace. The main γP line-broadening event occurs between 20 and 40 minutes of the reaction. Subsequently the line narrows, but not more than by 5%. The $W_{1/2}^{\beta P}$ trace of ATP shows more complex behavior; within 100 min it makes a full oscillation about the 0.26 ppm value (Fig. 5 βP-A). In the first 10–15 min, the βP resonance narrows by 10%. Between 20 and 40 min, it broadens by 20% (in concert with γP) and narrows again afterwards. During the first 40 min, the $W_{1/2}^{\beta P}$ value of caged ATP does not change; subsequently, it increases by 20% (SNR values between 2.1 and 19.8) (Fig. 5 βP-B). The αP resonances of caged and nascent ATP are separated by 0.3 ppm, which is only slightly larger than their linewidths. Thus, the fitted $W_{1/2}^{\alpha P}$ data are likely to be biased by the spectral overlap and will not be discussed.

The observed residual linewidth kinetics of β- and γP resonances can be interpreted in terms of weak hydrogen bonding **4a** ↔ **4c**; **5a**,**7a** ↔ **5c**,**7c**; **6a**,**7d** ↔ **6c**,**7e** and proton exchange between **7a**, **7d**, **7g**, **7f**, illustated in Scheme 1. The γP resonance can be additionally broadened by the fast proton exchange between the two almost identical oxygen anions at the γ-phosphate, **7g** ↔ **7g**.

Chemically exchanging **4a** and **4c** are formed in the course of the reaction. Their βP resonances overlap, which results in apparent line broadening. The δ_P values of the caged intermediates **1a–3a** are identical. Initially, the low-intensity, broad βP line of **4a,b** is hidden under the high-intensity, narrow βP signal of **1a–3a**. In the course of the photoreaction, the signal intensity of **1a–3a** decreases to the level of **4a,b**, from SNR = 86.4 to 19.8. As a result, the line broadening becomes apparent after ~50 min (Fig. 5 βP-B). Accordingly, chemical exchange **5a**,**7a** ↔ **5c**,**7c** can be observed only during the initial period of the reaction, when the product species **7e** are just being formed (SNR values between 2.9 and 33.2). After 10–20 min, the low-intensity broad βP signal of **7a**,**7c** is covered by the high-intensity, narrow βP resonance of **7e**, leading to the apparent narrowing of the line (Fig. 5 βP-A). The second βP line-broadening event occurs after 40–50 min of the reaction, during evolution of the protolytic equilibrium at **7a**, **7d**, **7g**, **7f** as the proton exhanges between the phosphates (Fig. 5 βP-A, γP-A). For the βP resonance of ATP, an additional exchange **6a**,**7d** ↔ **6c**,**7e** can be envisaged in the "post-reaction" hydrogen bonding between the keto-oxygen of **6c** and the βP-bound proton of **7e**, which would additionally contribute to the βP line broadening after 40–50 min of the reaction. The exchange vanishes as **6a** and **7d** diffuse from each other, and the βP line narrows again.

Conclusions

Chemical kinetics of the photoinduced intramolecular redox reaction of the adenosine-5′-triphosphate-[P^3-(1-(2-nitrophenyl)-ethyl)]ester (caged ATP, NPE-ATP) has been studied in frozen aqueous solution under conditions of continuous illumination by time-resolved ^{31}P LT MAS NMR spectroscopy. ATP with the ^{31}P resonances at −8.77 (γ), −13.05 (α) and −23.98 ppm (β) is formed with 100% yield from its caged precursor at −13.32 (α), −14.23 (γ) and −25.08 ppm (β) with an observed rate constant $k_1^{obs} = 2.4 \pm 0.2\ h^{-1}$ at 245 K. The reaction is accompanied by a release of the proton equivalent, which can be monitored by ^{31}P NMR as the induced shift of the phosphorus resonances of ATP. Analyses of the chemical shift and residual linewidth kinetics indicate that the NPE-phosphate ester bond is broken prior to the proton release, suggesting the involvement of the 1-hydroxy,1-(2-nitrosophenyl)-ethyl carbocation intermediate. The detailed kinetic analyses of the isotropic chemical shift, residual linewidth and intensity changes indicate that the initial light excitation step is followed by two parallel cascades of dark reactions interconnected by chemical equilibria. The photoactivation of caged ATP is accompanied by a pH jump, which, in the absence of the appropriate proton sink can reach several pH units. This has to be taken into account when using caged ATP in studies of the ATP-dependent enzymatic reactions. In many cases, protonation of the functional residues in the active site after cage release may modulate the catalytic properties of the enzyme.

Acknowledgements

The support of J. Hollander with the light-induced experiments is gratefully acknowledged. The research was supported by a VENI grant to A.V.C. (700.53.406) from the Netherlands Organization for Scientific Research (NWO). A.V.C. thanks G. Lodder and D. V. Fillipov for insightful discussions.

References

1 A. A. Beg, G. G. Ernstrom, P. Nix, M. W. Davis and E. M. Jorgensen, *Cell*, 2008, **132**, 149–160.
2 G. C. Ellis-Davies, *Nat. Methods*, 2007, **4**, 619–628.
3 A. Fibich, K. Janko and H. J. Apell, *Biophys. J.*, 2007, **93**, 3092–3104.
4 Z. G. Gao, B. Hechler, P. Besada, C. Gachet and K. A. Jacobson, *Biochem. Pharmacol.*, 2008, **75**, 1341–1347.
5 G. M. Grotenbreg, N. R. Roan, E. Guillen, R. Meijers, J. H. Wang, G. W. Bell, M. N. Starnbach and H. L. Ploegh, *Proc. Natl. Acad. Sci. U. S. A.*, 2008, **105**, 3831–3836.
6 M. Matsuzaki, G. C. Ellis-Davies and H. Kasai, *J. Neurophysiol.*, 2008, **99**, 1535–1544.
7 A. Momotake, *Seikagaku*, 2007, **79**, 1153–1158.
8 E. Pryazhnikov and L. Khiroug, *Glia*, 2008, **56**, 38–49.
9 M. Volgraf, P. Gorostiza, S. Szobota, M. R. Helix, E. Y. Isacoff and D. Trauner, *J. Am. Chem. Soc.*, 2007, **129**, 260–261.
10 Z. Zhang, G. Papageorgiou, J. E. Corrie and C. Grewer, *Biochemistry*, 2007, **46**, 3872–3880.
11 J. P. Colletier, A. Royant, A. Specht, B. Sanson, F. Nachon, P. Masson, G. Zaccai, J. L. Sussman, M. Goeldner, I. Silman, D. Bourgeois and M. Weik, *Acta Crystallogr., Sect. D*, 2007, **63**, 1115–1128.
12 B. L. Stoddard, B. E. Cohen, M. Brubaker, A. D. Mesecar and D. E. Koshland, Jr, *Nat. Struct. Biol.*, 1998, **5**, 891–897.
13 A. V. Cherepanov, E. V. Doroshenko, J. Matysik, S. de Vries and H. J. M. de Groot, *Proc. Natl. Acad. Sci. U. S. A.*, 2008, **105**, 8563–8568.
14 A. V. Cherepanov, E. V. Doroshenko, S. de Vries and H. J. M. de Groot, *Holland Research School of Molecular Chemistry (HRSMC) Symposium*, Amsterdam, The Netherlands, 2007.

15 A. V. Cherepanov, E. V. Doroshenko, S. de Vries, J. Matysik and H. J. M. de Groot, *Holland Research School of Molecular Chemistry (HRSMC) Symposium*, Amsterdam, The Netherlands, 2007.
16 M. C. Hopflinger, O. Andruchova, O. Andruchov, H. Grassberger and S. Galler, *J. Exp. Biol.*, 2006, **209**, 668–676.
17 J. Wakayama, T. Tamura, N. Yagi and H. Iwamoto, *Biophys. J.*, 2004, **87**, 430–441.
18 Y. E. Goldman, M. G. Hibberd, J. A. McCray and D. R. Trentham, *Nature*, 1982, **300**, 701–705.
19 B. Sot, F. von Germar, W. Mäntele, J. M. Valpuesta, S. G. Taneva and A. Muga, *Protein Sci.*, 2005, **14**, 2267–2274.
20 F. Moro, V. Fernandez-Saiz and A. Muga, *Protein Sci.*, 2006, **15**, 223–233.
21 J. A. Dantzig, H. Higuchi and Y. E. Goldman, *Methods Enzymol.*, 1998, **291**, 307–348.
22 H. Higuchi, E. Muto, Y. Inoue and T. Yanagida, *Proc. Natl. Acad. Sci. U. S. A.*, 1997, **94**, 4395–4400.
23 M. Stolz, E. Lewitzki, W. Mantele, A. Barth and E. Grell, *Biopolymers*, 2006, **82**, 368–372.
24 M. Krasteva and A. Barth, *Biochim. Biophys. Acta*, 2007, **1767**, 114–123.
25 T. Gropp, N. Brustovetsky, M. Klingenberg, V. Muller, K. Fendler and E. Bamberg, *Biophys. J.*, 1999, **77**, 714–726.
26 K. Agam, S. Frechter and B. Minke, *Cell. Calcium*, 2004, **35**, 87–105.
27 R. Dumollard, K. Hammar, M. Porterfield, P. J. Smith, C. Cibert, C. Rouviere and C. Sardet, *Development*, 2003, **130**, 683–692.
28 Y. V. Il'ichev and J. Wirz, *J. Phys. Chem. A*, 2000, **104**, 7856–7870.
29 K. Schaper, D. Dommaschke, S. Globisch and S. A. Madani-Mobarekeh, *J. Inf. Recording.*, 2000, **25**, 339–354.
30 S. Walbert, W. Pfleiderer and U. E. Steiner, *Helv. Chim. Acta*, 2001, **84**, 1601–1611.
31 R. S. Givens, M. B. Kotala and J.-I. Lee, in *Dynamic Studies in Biology*, ed. M. Goeldner and R. Givens, Wiley-VCH Verlag GmbH & Co. KGaA, Weinheim, Germany, 2005, pp. 95–129.
32 M. Schacht, N. Boukis, E. Dinjus, K. Ebert, R. Janssen, F. Meschke and N. Claussen, *J. Eur. Ceram. Soc.*, 1998, **18**, 2373–2376.
33 S. Biagini, M. Casu, A. Lai, R. Caminiti and G. Crisponi, *Chem. Phys.*, 1985, **93**, 461–473.
34 E. Daviso, G. Jeschke and J. Matysik, in *Biophysical Techniques in Photosynthesis, Volume II*, ed. T. J. Aartsma and J. Matysik, Springer Publishers, Dordrecht, 2008, vol. 26, pp. 385–399.
35 J. Matysik, Alia, J. G. Hollander, T. Egorova-Zachernyuk, P. Gast and H. J. de Groot, *Indian J. Biochem. Biophys.*, 2000, **37**, 418–423.
36 B. E. Fischer, U. K. Haring, R. Tribolet and H. Sigel, *Eur. J. Biochem.*, 1979, **94**, 523–530.
37 S. G. Brown, R. M. Hawk and R. A. Komoroski, *J. Inorg. Biochem.*, 1993, **49**, 1–8.
38 J. Choi and M. Terazima, *Photochem. Photobiol. Sci.*, 2003, **2**, 767–773.
39 K. Barabas and L. Keszthelyi, *Acta Biochim. Biophys. Acad Sci. Hung.*, 1984, **19**, 305–309.
40 A. Barth, K. Hauser, W. Maentele, J. E. T. Corrie and D. R. Trentham, *J. Am. Chem. Soc.*, 1995, **117**, 10311–10316.
41 J. A. McCray, L. Herbette, T. Kihara and D. R. Trentham, *Proc. Natl. Acad. Sci. U. S. A.*, 1980, **77**, 7237–7241.
42 D. T. Major, A. Laxter and B. Fischer, *J. Org. Chem.*, 2002, **67**, 790–802.
43 C. De Stefano, D. Milea, A. Pettignano and S. Sammartano, *Biophys. Chem.*, 2006, **121**, 121–130.
44 R. A. Alberty, R. M. Smith and R. M. Bock, *J. Biol. Chem.*, 1951, **193**, 425–434.
45 B. Geil, T. M. Kirschgen and F. Fujara, *Phys. Rev. B*, 2005, **72**, 014304.
46 R. S. Givens and L. W. Kueper, III, *Chem. Rev.*, 1993, **93**, 55–66.
47 R. S. Givens, B. Matuszewski, P. S. Athey and M. R. Stoner, *J. Am. Chem. Soc.*, 1990, **112**, 6016–6021.

